24th INTERNATIONAL CONGRESS ON SOUND AND VIBRATION
23–27 July 2017, London

ICSV24
23-27JULY 2017
LONDON CALLING

FINITE DIFFERENCE TIME DOMAIN SIMULATION OF HYBRID 1D/3D BRASS INSTRUMENT MODEL AND COMPARISON TO MEASURED RADIATION DATA

Reginald Langford Harrison, Brian Hamilton, and Amaya López-Carromero
University of Edinburgh, Acoustics and Audio Group, Edinburgh, UK
email: r.l.harrison-3@sms.ed.ac.uk

In this paper we present a hybrid brass instrument model consisting of two parts: a 1D wave propagation model for the slowly varying bore profile that includes viscous and thermal losses; and a 3D wave propagation model under rigid boundary termination for the bell section, allowing for lossless radiation into an open 3D space. These 1D and 3D models are simulated using Cartesian finite difference time domain (FDTD) methods and are coupled using principles of energy conservation. Comparisons are made with experimental measurements obtained from a linear microphone array.

Keywords: Musical acoustics, room acoustics, finite difference methods, FDTD

1. Introduction

The behaviour of a brass instrument is determined by the profile of the instrument's internal air column along with its interaction with the acoustic space. Modelling of brass and woodwind instruments has been primarily performed in one dimension (1D) with assumptions made about the types of waves that propagate (planar/spherical). These models are then terminated with a radiation impedance such as that presented by Levine and Schwinger [1].

Although these models are suitable for cylinders and tubes with slowly varying profiles, the one dimensional assumption begins to break down for tubes with a large flare as higher modes are excited across the wavefront. This is the case in the bell portion of brass instruments such as the trombone. Modelling the system in higher spatial dimensions, such as three dimensions (3D), would automatically include this mode transfer in the flaring sections of the instrument, but 3D simulations come at a cost. Modelling in higher dimensions increases the amount of computation required and also creates modelling issues when including boundary layer losses at the tube walls.

Instead of using one type of model, a hybrid approach can be used to take advantage of each systems strengths. The 1D models can be used in cylindrical and slowly varying portions of the instrument for fast computation and accurate representation of the boundary layer losses. The 3D model can then be used to model the flaring portion of the instrument where mode transfer occurs but boundary layer effects are less prominent. Noreland [2] first presented this type of approach by using a two-dimensional curvilinear finite-difference time-domain (FDTD) solver in curvilinear coordinates to calculate the radiation impedance of the bell of an instrument. This was then used to terminate a Transmission Line calculation of the impedance in the slowly varying portion of the instrument. This was later used in bore design approaches [3].

Because Noreland's approach to the FDTD solver involved using a curvilinear coordinate system that matched the walls of the instrument, cells that were further away from the throat of the horn get bigger. This reduces the available bandwidth of the system and negatively impacts the dispersion behaviour of the system. This is a problem in a sound synthesis setting as higher sample rates are required to overcome this problem.

A great deal of work has been performed using regular Cartesian grids to model wave propagation in rooms (e.g., [4]). Although these schemes still have issues with bandwidth and dispersion, they are constant throughout the space and are also amenable to parallel implementations to improve simulation speeds. We therefore use these grids to model the three-dimensional portion of the instrument.

The paper is structured as follows. The 1D and 3D parts of the problem are presented along with the coupling condition and comparisons are made between experiment and a simulation using only 1D propagation. A method for measuring the radiation behaviour using a microphone array is described and experimental measurements are compared to simulations in the 3D field. Finally, concluding remarks are made about auralisation of instruments in real acoustic spaces.

2. The model

A method for coupling a 1D acoustic tube to a 3D air box was described in [5] but this only considered the interface between the systems and not modelling any of the bore profile in the 3D space. Here, we briefly describe the lossless system along with numerical method for solving this system; more information on the use of FDTD methods can be found in various texts (e.g., [6]). Losses are added to the 1D system using the method described in [7] using a fourth-order filter.

2.1 The system

Our hybrid instrument system consists of a 1D acoustic tube connected to a 3D air box via a surface Ω. This surface is equal to the cross-sectional area at the end of the 1D tube; see Fig. 1.

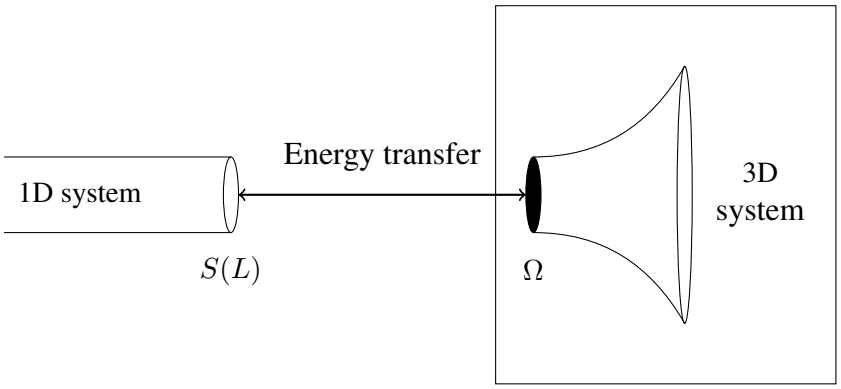

Figure 1: Schematic of the hybrid acoustic tube system. The section with slowly varying bore is modelled in 1D and the flaring section is modelled in 3D. Energy is transferred from the 1D system to the 3D system via the surface Ω.

Dynamics of a lossless acoustic tube are given by the horn equation, which, in first order form, is

$$\frac{S}{\rho c^2}\partial_t p = -\partial_z \left(Sv\right), \quad \rho \partial_t v = -\partial_z p \tag{1}$$

where $p(t,z)$ is the acoustic pressure, $v(t,z)$ is the particle velocity, ρ is the air density, c is the speed of sound, and $S(z)$ is the cross-sectional area of the tube. The symbols t and z denote time and axial coordinate so $t \in \mathbb{R}^+$ and $z \in [0, L]$, where L is the length of the tube. Partial derivatives are denoted by the symbol ∂, with the subscript giving the variable the derivative is taken with respect to.

Lossless wave propagation in 3D is given by the wave equation

$$\partial_{tt}\psi - c^2\nabla^2\psi = 0 \tag{2}$$

where $\psi(t,x,y,z)$ is the acoustic velocity potential and $\nabla^2 = \partial_{xx} + \partial_{yy} + \partial_{zz}$ is the Laplacian operator. The axial position coordinate is aligned with the coordinate z in 3D, with x and y defining a plane orthogonal to z.

Pressure and velocity are related to the acoustic velocity potential by

$$p_{3D} = \rho \partial_t \psi, \quad \mathbf{v}_{3D} = -\nabla \psi \tag{3}$$

where ∇ is the gradient vector operator.

The tube wall can be set as a boundary condition in the 3D system. This is done with a zero velocity condition so that $\mathbf{n} \cdot \nabla \psi = 0$ on the tube wall with outward normal vector $\mathbf{n}$. Anechoic wall terminations can be included using absorbing boundary conditions [8].

2.2 Finite-difference method

A pair of interleaved grids are used to model wave propagation within the acoustic tube so that $p_l^n = p(lh_1, nk)$ and $v_{l+1/2}^{n+1/2} = v((l+1/2)h_1, (n+1/2)k)$, where n and l are integers. The time step is denoted by k and h_1 is spatial step size of the 1D grid. The velocity potential is sampled on a single grid so that $\psi_{\mathbf{l}}^{n+1/2} = \psi(\mathbf{l}h_3, (n+1/2)k)$, where $\mathbf{l} = [l_x, l_y, l_z]$, l_x, l_y, and l_z are integers, and h_3 is the step size of the 3D grid.

Examples of temporal and spatial shifting operations and their actions are

$$e_{t\pm} p_l^n = p_l^{n\pm1}, \quad e_{z\pm} p_l^n = p_{l\pm1}^n, \quad e_{x\pm} \psi_{l_x,l_y,l_z}^{n+1/2} = \psi_{l_x\pm1,l_y,l_z}^{n+1/2} \tag{4}$$

These are used to construct approximations to the partial derivatives such as

$$\partial_t \approx \delta_{t\pm} = \frac{e_{t\pm} \pm 1}{k}, \quad \partial_t \approx \delta_{t\cdot} = \frac{e_{t+} - e_{t-}}{2k}, \quad \partial_{tt} \approx \delta_{tt} = \delta_{t+}\delta_{t-} \tag{5a}$$

$$\partial_z \approx \delta_{z\pm} = \frac{e_{t\pm} \pm 1}{h}, \quad \partial_{zz} \approx \delta_{zz} = \delta_{z+}\delta_{z-} \tag{5b}$$

and similarly for derivatives in the x and y directions. Note that the spatial derivatives will use different step sizes for the two systems: $h = h_1$ for the 1D system, $h = h_3$ for the 3D system. Averaging operators are given by

$$\mu_{t+} = \frac{e_{t+} + 1}{2}, \quad \mu_{z-} = \frac{1 + e_{z-}}{2} \tag{6}$$

2.3 Discrete system

The discrete form of the horn equation is given by

$$\rho \delta_{t-} v_{l+1/2}^{n+1/2} + \delta_{z-} p_l^n = 0, \quad \frac{\bar{S}_l}{\rho c^2} \delta_{t+} p_l^n + \delta_{z-} \left(S_{l+1/2} v_{l+1/2}^{n+1/2} \right) = 0 \tag{7}$$

The discrete wave equation is given by

$$\delta_{tt} \psi_{\mathbf{l}}^{n+1/2} - c^2 \left(\tilde{\delta}_{xx} + \tilde{\delta}_{yy} + \tilde{\delta}_{zz} \right) \psi_{\mathbf{l}}^{n+1/2} = 0 \tag{8}$$

Here, $\tilde{\delta}$ represents the Laplacian terms that have been modified to include the instrument bell. The bell is included using discrete Neumann conditions on a Cartesian grid (see, e.g., [4, Chapter 3]).

Energy is transferred between the acoustic tube at $l = N$ and the discrete surface Ω_d in the air box. Assuming that pressure is constant on this surface and volume flow is conserved, the following boundary conditions hold

$$\rho \delta_{t\cdot} \mathbf{\Psi}_{\Omega_d} = \mathbf{q} \mu_{t+} p_N, \quad \mu_{z-} \left(S_{N+1/2} v_{N+1/2} \right) = \mathbf{q}^T \delta_{z-} \mathbf{\Psi}_{\Omega_d} \tag{9}$$

where $\mathbf{\Psi}_{\Omega_d}$ is a vector that stores the values of the velocity potential on the surface Ω_d and $\mathbf{q}$ is a column vector of ones of size $N_\Omega \times 1$, N_Ω is the number of elements on the surface Ω_d, and ^{T} denotes the transpose operator.

From these boundary conditions, the following update can be derived via manipulation of the difference operators

$$\mathbf{A} \begin{bmatrix} \mu_{t+} p_N^n \\ \mu_{z-} \left(S_{N+1/2} v_{N+1/2}^{n+1/2} \right) \end{bmatrix} = \mathbf{B} \tag{10}$$

where

$$\mathbf{A} = \begin{bmatrix} \frac{2\bar{S}_N}{\rho c^2 k} & \frac{2}{h_1} \\ \frac{2N_\Omega}{c^2 k} & -\frac{\rho}{h_3^3} \end{bmatrix} \tag{11a}$$

$$\mathbf{B} = \begin{bmatrix} \frac{2\bar{S}_N}{\rho c^2 k} p_N^n + \frac{2}{h_1} S_{N-1/2} v_{N-1/2}^{n+1/2} \\ \rho \mathbf{q}^T \left(\frac{2}{c^2 k} \delta_{t-} + \delta_{xx} + \delta_{yy} + \frac{1}{h_3} \delta_{z+} \mathbf{\Psi}_{\Omega_d}^{n+1/2} \right) \end{bmatrix} \tag{11b}$$

Due to the discrete nature of the 3D grid, the surface Ω_d uses a staircased approximation to fit the surface area at the end of the acoustic tube [9]. It can be shown that the entire system, with absorbing boundaries, conserves energy (to machine precision) [7, 5, 4].

3. Simulation results for a full instrument

Simulations of the trumpet with mouthpiece were performed in MATLAB, at a sample rate of 100 kHz for one second duration. The interface between the 1D and 3D models was set at 1.3 m, meaning that the final 0.08 m of the trumpet were modelled in the 3D space—this is where the flare of the instrument becomes strong. The 3D box was a cube of side length 0.5 m terminated with first-order absorbing boundary conditions [8]. Comparisons were made with the same 1D acoustic tube model model terminated with a RLC network approximation to the Levine and Schwinger radiation impedance [10, 11]. Both 1D models used the same interior loss model, although the embedded system is lossless in the 3D section.

Experimental measurements of the input impedance were made using the BIAS measurement system [12]. Results are presented in Fig. 2.

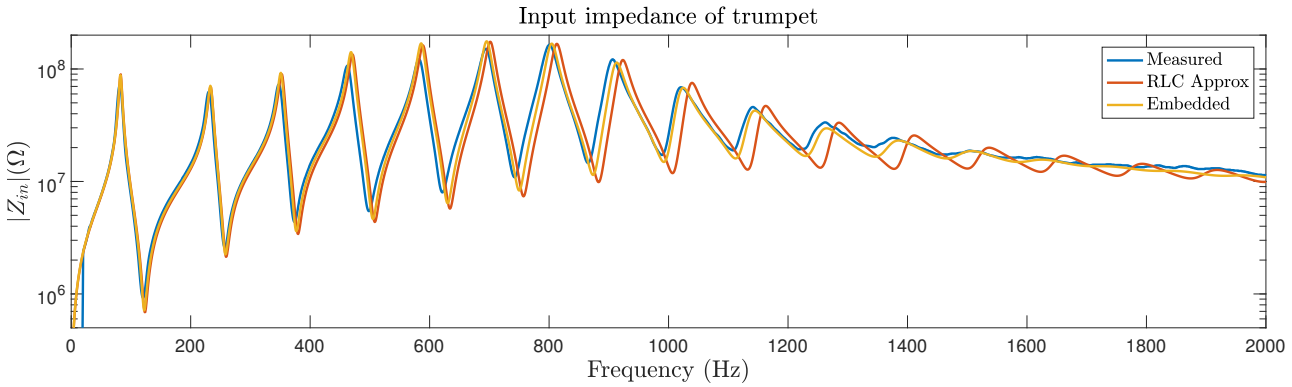

Figure 2: Input impedance for a trumpet. Measured impedance (blue), FDTD simulation terminated with a RLC approximation to the radiation impedance of Levine and Schwinger (red), and FDTD simulation of embedded system (yellow).

The first five impedance peaks are similar for both simulations which is to be expected as the behaviour is this frequency range is dominated by boundary layer losses. The higher peak behaviour differs, with the embedded system peaks matching experimental measurements better than the system terminated with the RLC radiation impedance. Above 1200 Hz, the simulation terminated with the RLC model still exhibits peaks, whereas in the experiments and the embedded simulation results the peaks become less present. This is because as the trumpet bore profile begins to flare, the waves become more spherical—behaviour which is modelled in the embedded system.

4. Microphone array measurements

The radiation field of a trombone horn was measured using a microphone array; see Fig. 3. The array consisted of 23 1/4" Roga RG-50 microphones mounted perpendicularly to the instrument axis and its distance from the instrument could be adjusted using an Arduino stepper motor.

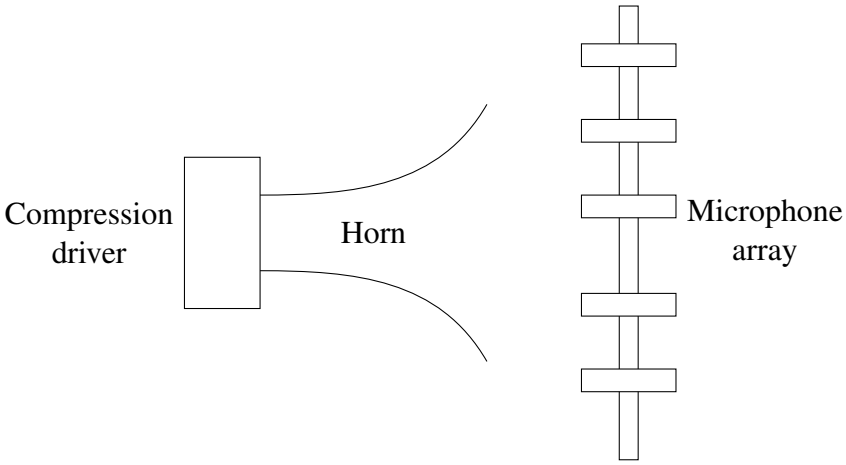

Figure 3: Schematic of experimental set up.

The instrument was excited using an exponential sweep from 10 Hz to 20 kHz over 40 s using a Visaton DR 45 N compression driver. Signals were recorded using the array at intervals of 12 mm from the end of the instrument up to 1020 mm. A Meggit 8507C-2 piezoresistive pressure transducer was placed within the throat of the horn as a reference to what the compression driver was producing. Distortion produced by the compression driver was removed from the recorded signals using the method described by Farina [13].

5. Comparison to 3D FDTD simulations

The experimental measurements are compared to simulations performed in the 3D field using a trombone horn. Simulations are performed at a sample rate of 80 kHz ($h_3 \approx 7.45$ mm) in a box of dimensions 1.5 m$\times$1 m$\times$1 m. In the simulations, the throat of the horn is excited with a 4 kHz sinusoid and simulations are allowed to run until the entire field has been excited and patterns in the radiation field can be observed. Numerical results, alongside experimental results for the same frequency, are displayed in Fig. 4. Aside from a linear offset and scaling factor, general agreements can be observed between the displayed radiation profiles, both in the near and far field. Measurements appear to show a higher directionality, but this could be due to calibration and warrants further study. See Fig. 5 for a 2D snapshot of the same pressure field, including the bell profile. Note the diffraction effects around the bell.

6. Concluding remarks

We have presented simulations that have modelled the behaviour of brass musical instruments. This hybrid 1D/3D model allows for more accurate modelling of the radiation field than purely 1D simulations (or 2D simulations, for that matter). Simulation of input impedances and radiation profiles have been carried out and compared to experimental data, showing general agreement between numerical and experimental data.

It is useful to point that all of the simulations were performed using a personal desktop machine in MATLAB. The trumpet input impedances took under 25 minutes using a 2013 MacBook Pro for a one second simulation at 100 kHz. The high sample rate was chosen so that the mouthpiece, which was particularly shallow for this instrument, could be accurately represented. For audio synthesis purposes lower sample rates could be used with shorter simulation times. There is much scope for optimisation using C/C++ implementations as well as parallelisations with graphics processing units (GPU). Real-time applications of a Cartesian 2D system have been achieved using GPUs [15], although it is important to note that the hybrid system presented here is more sophisticated in the modelling of boundary layer losses, the radiation field, and numerical stability of the system as a whole.

It is worth remarking that in terms of purely 1D models, one can, of course, improve accuracy by using a conical or curvilinear coordinate system, but discrete implementations of these systems, such as digital waveguides, have issues with stability for certain horn profiles [14].

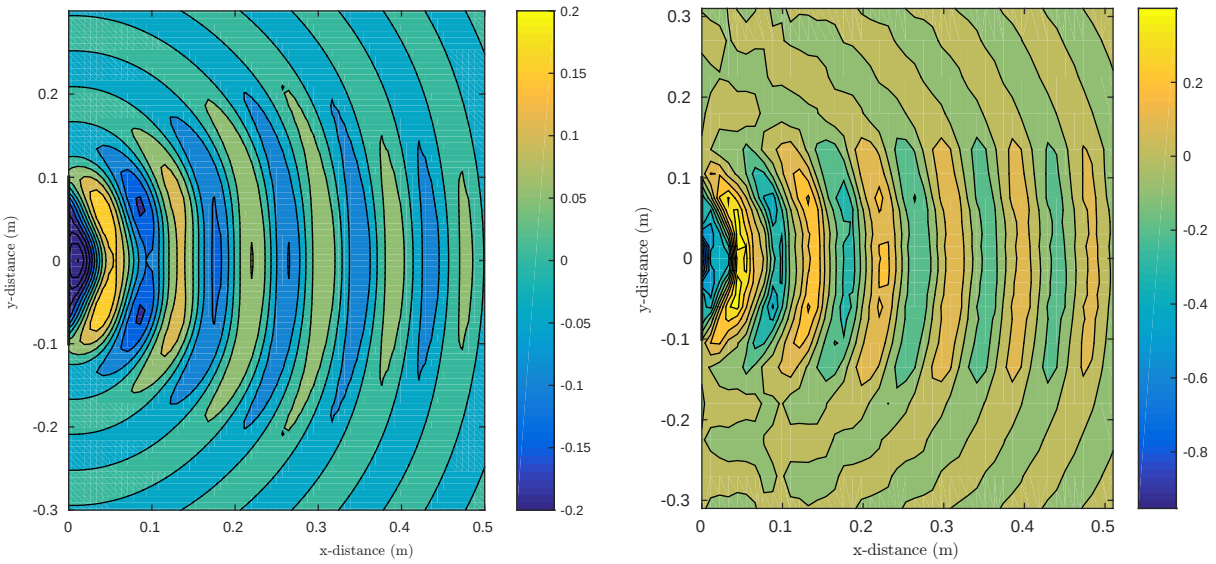

(a) simulated (b) measured

Figure 4: Simulated and experimentally measured pressure radiation field captures (in Pa.) for a 4 kHz sinusoidal input to a trombone along 2D plane. The x- and y-distances are measured from the centre of the bell-end. In this case, the radius of the bell-end is approximately 10 cm.

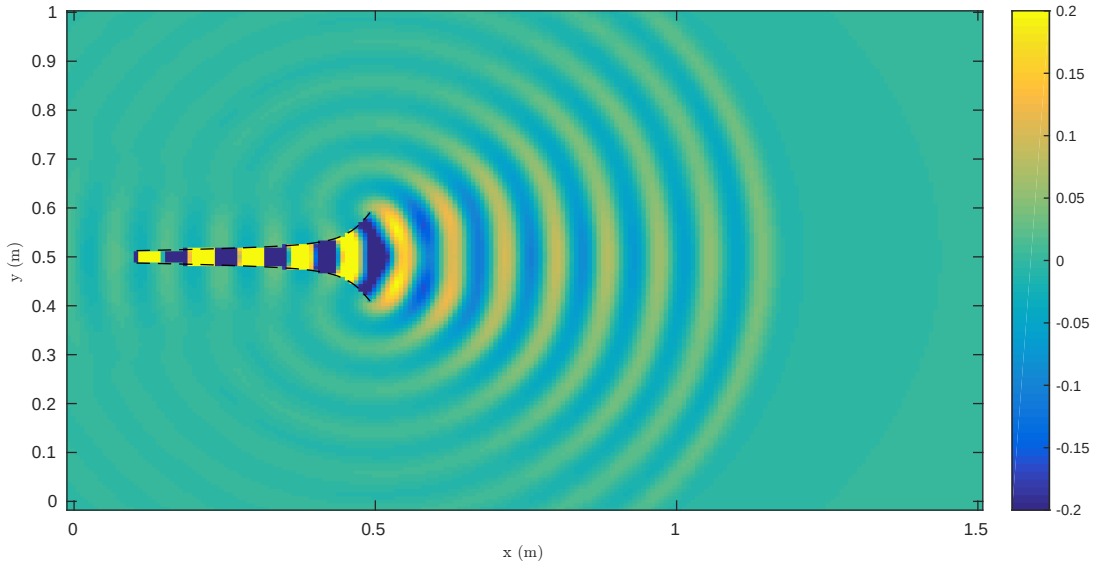

Figure 5: 2D snapshot of simulated 3D pressure field (in Pa.) for a 4 kHz driving sinusoid, showing only the 3D section of the trombone horn. Note that in this image, colours are saturated inside the bell due to higher pressure amplitudes.

The 1D model can be extended to include an excitation mechanism such as a lip reed, and methods of modifying the overall bore length by including valves (as seen in a trumpet) building on work presented in [17]. The 3D model can be extended from an anechoic environment to a concert hall by using a larger domain, and frequency-dependent losses in air and at walls [16]. Although using a Cartesian grid requires the use of a staircased approximation to the bell, the grid spacing used in the simulations is constant whereas Noreland's work [2] used a grid spacing that varied over the domain, reducing available available bandwidth of the simulation. Improved FDTD schemes for the 3D system could also improve the dispersion properties in this system.

7. Acknowledgements

Thanks to Arnold Myers and John Chick for providing instrument measurements. This work was supported by European Research Council under grant numbers ERC-2011-StG-279068-NESS and PoC-2016-737574-WRAM and the People Programme (Marie Curie Actions) of the European Unions Seventh Framework Programme FP7/2007-2013/ under REA grant agreement No. 605867 supporting the BATWOMAN ITN Project.

REFERENCES

1. Levine, H. and Schwinger, J. On the radiation of sound from an unflanged circular pipe, *Physical Review*, **73** (4), 383–406, (1948).
2. Noreland, D. A numerical method for acoustic waves in horns, *Acta Acustica united with Acustica*, **88**, 576–586, (2002).
3. Noreland, J. O. D., Udawalpola, M. R. and Berggren, O. M. A hybrid scheme for bore design optimization of a brass instrument, *Journal of the Acoustical Society of America*, **128** (3), 1391–1400, (2010).
4. Hamilton, B., *Finite Difference and Finite Volume Methods for Wave-Based Modelling of Room Acoustics*, Ph.D. thesis, The University of Edinburgh, (2016).
5. Harrison, R. and Bilbao, S. Coupling of a one-dimensional acoustic tube to a three-dimensional acoustic space using finite-difference time-domain methods, *Proceedings of the International Symposium on Musical and Room Acoustics*, La Plata, Argentina,, (2016).
6. Strikwerda, J. C., *Finite Difference Schemes and Partial Differential Equations: Second Edition*, Society for Industrial and Applied Mathematics (2004).
7. Bilbao, S. and Harrison, R. Passive time-domain numerical models of viscothermal wave propagation in acoustic tubes of variable cross section, *The Journal of the Acoustical Society of America*, **140** (1), (2016).
8. Engquist, B. and Majda, A. Absorbing boundary conditions for the numerical simulation of waves, *Mathematics of Computation*, **31** (139), 629–651, (1977).
9. Bilbao, S., Hamilton, B., Botts, J. and Savioja, L. Finite volume time domain room acoustics simulation under general impedance boundary conditions, *IEEE/ACM Transactions on Audio, Speech, and Language Processing*, **24** (1), 161–173, (2016).
10. Silva, F., Guillemain, P., Kergomard, J., Mallaroni, B. and Norris, A. N. Approximation formulae for the acoustic radiation impedance of a cylindrical pipe, *Journal of Sound and Vibration*, **322**, 255–263, (2009).
11. Bilbao, S. and Chick, J. Finite difference time domain simulation for the brass instrument bore, *Journal of the Acoustical Society of America*, **134** (5), 3860–3871, (2013).
12. Widholm, G. Brass wind instrument quality measured and evaluated by a new computer system, *Proceedings of the* 15^{th} *International Congress on Acoustics*, Trondheim, Norway, (1995).
13. Farina, A. Simultaneous measurement of impulse response and distortion with a swept-sine technique, *Audio Engineering Society Convention 108*, Feb, (2000).
14. Mignot, R., Hélie, T. and Matignon, D. Acoustic modelling of a convex pipe adapted for digital waveguide simulation, *Proceedings of the* 13^{th} *International Conference on Digital Audio Effects*, Graz, Austria, September, (2010).
15. Allen, A. and Raghuvanshi, N. Aerophones in flatland: Interactive wave simulation of wind instruments, *ACM Trans. Graph.*, **34** (4), 134:1–134:11, (2015).
16. Bilbao, S. and Hamilton, B. Wave-based room acoustics simulation: Explicit/implicit finite volume modeling of viscothermal losses and frequency-dependent boundaries, *Journal of the Audio Engineering Society*, **65** (1/2), 78–89, (2017).
17. Harrison, R.L., Bilbao, S., Perry, J., and Wishart, T.. An environment for physical modeling of articulated brass instruments. *Computer Music Journal*, **29** (4):80–95, (2015).